Omega-Shaped Inchworm-Inspired Crawling Robot With Large-Index-and-Pitch (LIP) SMA Spring Actuators

Je-Sung Koh, *Student Member, IEEE*, and Kyu-Jin Cho, *Member, IEEE*

***Abstract*—This paper proposes three design concepts for developing a crawling robot inspired by an inchworm, called the Omegabot. First, for locomotion, the robot strides by bending its body into an omega shape; anisotropic friction pads enable the robot to move forward using this simple motion. Second, the robot body is made of a single part but has two four-bar mechanisms and one spherical six-bar mechanism; the mechanisms are 2-D patterned into a single piece of composite and folded to become a robot body that weighs less than 1 g and that can crawl and steer. This design does not require the assembly of various mechanisms of the body structure, thereby simplifying the fabrication process. Third, a new concept for using a shape-memory alloy (SMA) coil-spring actuator is proposed; the coil spring is designed to have a large spring index and to work over a large pitch-angle range. This large-index-and-pitch SMA spring actuator cools faster and requires less energy, without compromising the amount of force and displacement that it can produce. Therefore, the frequency and the efficiency of the actuator are improved. A prototype was used to demonstrate that the inchworm-inspired, novel, small-scale, lightweight robot manufactured on a single piece of composite can crawl and steer.**

***Index Terms*—Anisotropic friction, composite, origami, printable robot, shape-memory alloy (SMA) spring actuator, smart composite microstructures (SCMs), soft robot, two-anchor crawling.**

I. Introduction

MANY researchers have developed various robots with novel gaits that can travel on rough terrains where conventional vehicles or other robots cannot. Most of these robots have been inspired by living organisms in nature. The locomotion of an organism can sometimes provide a suitable solution to overcome mobility limitations in hazardous situations.

Manuscript received November 14, 2011; revised March 19, 2012 and July 20, 2012; accepted July 24, 2012. Date of publication August 15, 2012; date of current version January 10, 2013. Recommended by Technical Editor A. Menciassi. This work was supported by the Research Center Programs through the National Research Foundation of Korea, funded by the Ministry of Education, Science and Technology under Grant 2009-0087640, Grant 2009-0082824, and Grant 2009-0070058.

The authors are with the Biorobotics Laboratory, School of Mechanical and Aerospace Engineering/Seoul National University Institute of Advanced Machinery and Design (SNU-IAMD), and Advanced Institutes of Convergence Technology, Seoul National University, Seoul 151-744, Korea (e-mail: kjs15@snu.ac.kr; kjcho@snu.ac.kr).

This paper has supplementary downloadable material available at http://ieeexplore.ieee.org, provided by the author. The material consists of a video showing four previous versions of the inchworm robot (Omegabot) prototypes and the current version of Omegabot. The size of the video is 23.06 MB. Contact kjcho@snu.ac.kr for further questions about this work.

Color versions of one or more of the figures in this paper are available online at http://ieeexplore.ieee.org.

Digital Object Identifier 10.1109/TMECH.2012.2211033

Fig. 1. Inchworm on a millimeter scale. An inchworm climbing (upper right), steering (middle right), and standing (lower right).

Worms such as the caterpillar of a moth are organisms that have a novel gait that enable them to propel through various environments. A worm is very slow and inefficient in terms of the energy used [1]. However, simple worm locomotion maintains mobility across various environments. Caterpillar locomotion can be categorized into two types: peristaltic crawling and two-anchor crawling. An earthworm, for example, performs peristaltic crawling motion by sequential contraction of segments. This locomotion is advantageous for specific movements such as burrowing or passing through a narrow gap. A few robots based on this motion have been developed to penetrate through narrow areas. These robots use various materials and mechanisms to build earthworm locomotors such as a polymer body and shape-memory alloy (SMA) coil actuators [2], [3], a metal-based body and motor [4], [5], and piezoelectric actuators [6]. The second type of caterpillar locomotion is two-anchor crawling, which can be observed in inchworms. Fig. 1 shows an inchworm with a 4-cm-long body. An inchworm is commonly a caterpillar of *geometrid* moths. Its structure is extremely simple, consisting of a cylindrical tube shape that can be bent. Even with this simple structure, the inchworm can climb a vertical surface and crawl on a narrow stick using prolegs, which are the small legs of a caterpillar. Furthermore, some species are able to roll and jump [7]. With this simple locomotion, i.e., the ability to bend its body into an "omega" shape, the inchworm can travel through small cracks and on leaves and branches. It can move in a 3-D space by bending its body in various directions. Crawling is an in-plane motion; however, by bending its body, it can move out of the plane and directly move to other points in the 3-D space. Some inchworm robots have been developed,

inspired by the high mobility of inchworms in 3-D space, such as [8] and [9], which use magnets or suction pads for adhesion. However, magnets and suction pads are limited by surface materials and conditions for adhesion.

On a small scale, simple locomotion of an inchworm robot may have many advantages in terms of a reduction in both the weight and the number of components. On the basis of the advantages of the simple crawling mechanism of an inchworm, a piezo-based inchworm robot was developed using a single piezo body structure [10]. Lin *et al.* [11] demonstrated a caterpillar robot that was composed of a soft polymer body structure, a simple gripper, and an SMA spring actuator. Kim *et al*. [12] show the inchworm robot using SMA embedded composite structure. The complexity of the robot system can be reduced using the SMA spring actuator and the anisotropic friction pad.

We previously developed robots inspired by the inchworm's omega-shaped crawling motion. These robots were built from a composite structure with flexure joints [13] and an SMA spring actuator. They do not employ metal-based pins and link joints that cause large friction losses at the microscale level. Instead, in these robots, flexible polymer films and composites replace the pins and metal links. Three-dimensional microrobot structures, e.g., microflying insect robots [14], flea-inspired jumping robot [15], are made from 2-D patterns. SMA has high energy density and a unique two-phase (martensite/austenite) property. Using these characteristics, SMA has been used for robotic hands [16], robotic fish fins [17], and crawling microrobots [18]. The previous versions of the Omegabot prototypes, [19]–[21], were an inchworm robot that could crawl using a composite structure and an SMA spring actuator. These previous designs contributed to the development of various mechanisms for improving the agility of robots. However, the previous versions of robots have various limitations such as a highly redundant degree of freedom (DOF) of the body structure and nonoptimized actuator design.

In this paper, we present an improved design of the Omegabot that concentrates on crawling and steering. The new inchworm robot is made of a single piece of composite that folds into four-bar mechanisms and a spherical six-bar mechanism and is actuated by a novel large-index-and-pitch (LIP) SMA spring actuator. The robot bends its body into the shape of an omega (Ω) using the two four-bar linkages for crawling, and it bends its body orthogonal to the crawling direction using the spherical six-bar linkage for steering. Compared with the previous versions of the Omegabot, in the case of the proposed Omegabot, the four-bar mechanisms reduce the DOFs of the robot to minimize redundant motion, which causes unpredictable motion by the external force. The anisotropic friction pads are attached to the bottom of the head and the tail segments; these anchor the head segment while the tail segment is being pulled forward during folding, as well as anchor the tail segment while the head segment is being pushed forward during unfolding. We propose the use of an LIP SMA spring actuator to improve the actuation speed and efficiency in cyclic actuation. The proposed Omegabot is approximately 150 mm long, can crawl at a speed of 10 mm/s, and can steer at a speed of 110°/min. This research provides guidelines for designing a lightweight inchworm robot on a composite using SMA spring actuators. The unique design of the mechanisms on the composite enabled the robot to be lightweight. The resulting lightweight crawling robot can be transported in microair vehicles to areas where there is need for sensing and reconnaissance.

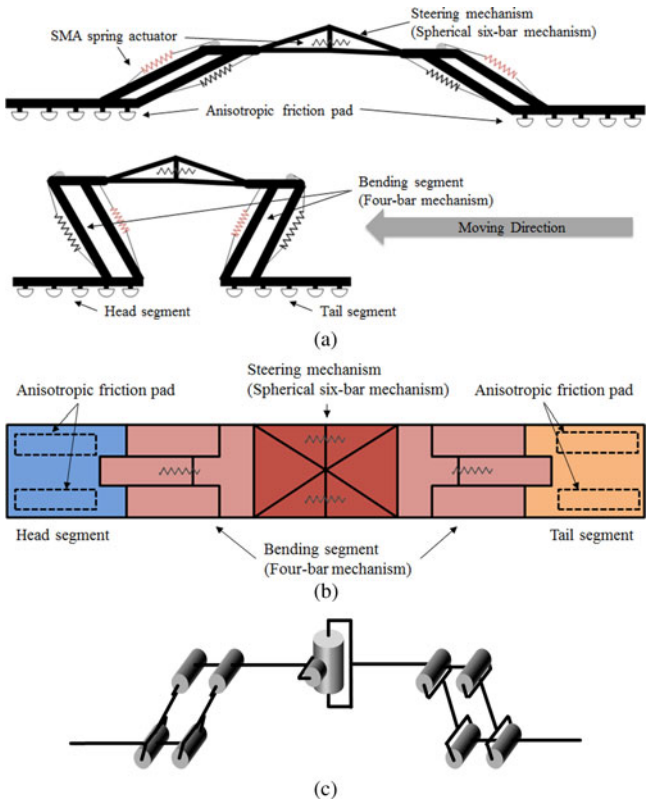

Fig. 2. (a) Schematic design of the Omegabot. Red coil indicates the activated actuator. (b) Schematic design (top view), different colors indicate corresponding segments. (c) Illustration converted into links and joints. The structure has four-bar linkages at each side of steering joint, which is perpendicular rotation axis to bending axis of four-bar linkages.

II. Inchworm Robot Design

The Omegabot's mechanical design is based on segmented rigid structures, whereas a real inchworm is soft-bodied and has no rigid skeleton. A soft body has infinite DOFs. To reduce the total DOFs and produce crawling locomotion with an omega-shaped bending motion, the robot is segmented by rigid links consisting of four-bar linkages and a steering mechanism. The omega bending motion amplifies the stride length by bending the segments, whereas other types of worms using peristaltic motion extend and contract their segments. As shown in Fig. 2, two four-bar linkages, called the bending segments, are symmetrically attached to each side of the steering mechanism. Each bending segment has one DOF and produces Z-shaped bending. The bending segments lift the middle part of the robot and pull the head and tail segments toward the center of the robot. Each four-bar mechanism provides the minimum DOF for the omega bending motion. The steering mechanism is a spherical six-bar linkage that has three DOFs (yaw, pitch, and roll). The yaw angle is controlled actively and determines the direction of crawling,

whereas the pitch and roll angles are determined passively by the lowest elastic-energy position. These passive DOFs allow the robot to adapt to its environment. With these two four-bar linkages and one spherical six-bar linkage, the robot produces contraction, extension, and steering bending motions.

The next essential component of the robot is the anisotropic friction pads. Anisotropic friction pads are patterned structures that have different friction coefficients depending on the direction of the lateral force. They are designed to always have larger forward-friction forces than backward-friction forces. For a friction-based inchworm robot to move, the forward static-friction coefficient must be larger than the backward static-friction coefficient. When the feet of the robot satisfy this single requirement, the robot moves forward with simple inchworm motion; when the robot contracts, the head segment is fixed on the ground due to the large forward friction while the tail segment slides due to the small backward friction. The direction of the friction is inverted when the robot extends. The forward friction force is always larger than the backward friction due to the anisotropic friction pads. Therefore, the robot moves forward with this simple locomotion.

The last important component is the actuator. We propose an SMA coil-spring actuator that has a large spring index and a large pitch angle (LIP SMA spring actuator) to increase the speed of the actuator. In a small-scale robot, the volume and mass of the actuator are limited by the size of the robot. A small robot requires a small actuator with high power density and a simple structure. SMA coil actuators meet these requirements, although they have some disadvantages in terms of control and thermal properties. The proposed LIP SMA spring actuator enhances the cooling of the actuator, thereby increasing the speed, by operating the actuator in a range that is not normally used. The actuators are attached antagonistically to the four-bar linkages, as shown in Fig. 2(a). The actuator attached above the bending segment unfolds the robot body, and two actuators attached under the segment folds the robot body. The two upper SMA actuators and four lower SMA actuators are electrically connected in series with the embedded wiring. Each series of SMA actuators is activated alternately. In the steering mechanism, two SMA actuators are attached to each side of the mechanism. The robot turns toward the direction of the activated actuator.

A. Four-Bar Linkage

The four-bar linkage mechanism has a single DOF for producing a "Z" shape (half shape of the omega). The symmetrical attachment of two four-bar linkages generates the omega shape. In this section, we present the 2-D pattern design of the four-bar linkage for composite manufacturing. The robot body structure is fabricated with glass-fiber composite and flexible-film joints. This fabrication process requires a 2-D pattern design for laser machining. The 2-D pattern becomes a 3-D structure by folding. Assembling a small-scale robot with small parts is very difficult and requires high-precision manipulation. Therefore, to reduce the requirements for the assembly process, we designed the four-bar linkage on a single piece of composite plate that can be fabricated from a single cut and that does not require assembly, as shown in Fig. 3. With this integrated structure design, assembly by hand, such as bonding, is not required for the robot body, although attachment of the actuators and the wiring still requires bonding. This process is similar to origami, an art of paper folding, since a 3-D shape can be built by just folding a sheet.

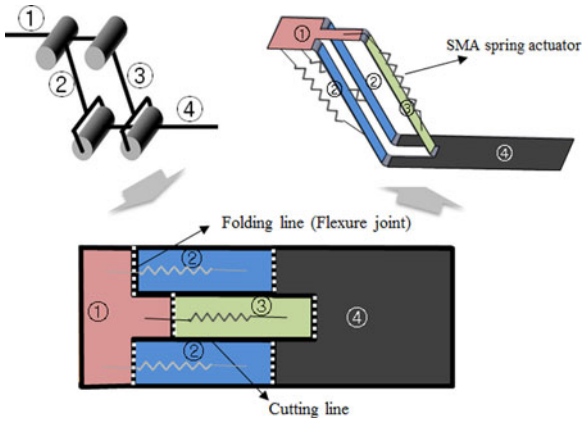

Fig. 3. Two-dimensional design of the four-bar linkage. On a single piece of composite, plane links and flexure joints are patterned through cutting and folding line. Two-dimensional pattern is folded into four-bar linkage. SMA spring actuators are attached at upper side and lower side of the composite. (In lower figure, gray spring line: SMA spring attached beneath the segment; black spring line: SMA spring attached above the segment.)

The numbers on the links in Fig. 3 indicate the corresponding links of the conventional four-bar linkage. The length of the four-bar linkage (bending segment) is an important parameter for robot performance, i.e., stride length and robot speed. For two-anchor crawling, the middle part (two four-bar linkages and steering joint) moves up and down repeatedly. The longer bending segment induces longer stride length and higher robot speed. In the current version of the robot, the length of the bending segment length is set to be 25 mm, which is the maximum value that prevents rollover of the robot during steering. As shown in Fig. 2, the bending segment is designed to bend from 60° to 120°. This value is verified from experimental results as well (see Table II). The 60° bending angle guarantees that the bending segments do not interfere with each other during contraction and the SMA actuators are not obstructed by the bending segment. In order to bend the bending segment 60°, actuators are required to produce a displacement of 3 mm. Since the length of the bending segment is 25 mm, the end segment moves by 25 mm for each contraction. The energy analysis with normalized segment lengths can be a more general issue of the inchworm-inspired crawling robot including Omegabot. In this paper, we focus on structure and actuator design.

B. Steering Mechanism

Another bending axis, one that is orthogonal to the bending axis for crawling, is required for the inchworm robot to turn while it crawls forward. Pitch-axis bending generates a forward movement, whereas yaw-axis bending generates a turning motion. A universal joint provides a suitable additional bending axis. However, from a practical viewpoint, the steering joint

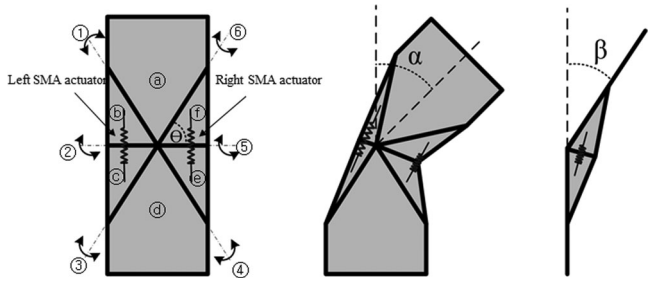

Fig. 4. Pattern design of the spherical six-bar linkage used as a steering mechanism. (θ: shape angle, α: steering angle (yawing motion of the mechanism), β: angle of the pitching motion.)

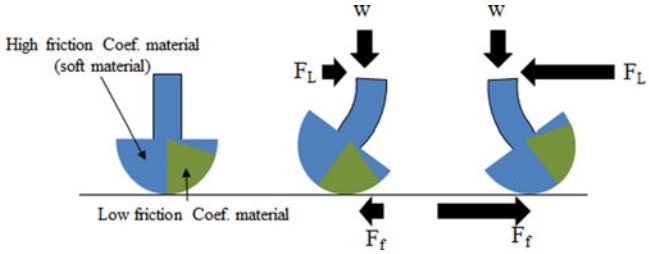

Fig. 5. Anisotropic friction mechanism. Depending on the direction of the lateral force, the beam bends, changing the side of the material that touches the ground. (w: normal force (weight of the robot), F_L: lateral force, F_f: friction force.)

should be built on a small scale using a 2-D composite manufacturing process. Several mechanical elements are designed as 2-D patterns for laser machining. For example, a sarrus linkage built from a 2-D pattern can replace a prismatic joint [18], and a spherical five-bar linkage built from a 2-D pattern is used in a microflying robot to change the angle of attack of the robot's flapping wings [13].

For steering purposes, we propose a spherical six-bar linkage. As shown in Fig. 4, it has six links (rigid plates) and six bending axes (flexure joints) intersecting at the center point, all on a 2-D plane. The spherical six-bar linkage can generate pitch-axis motion and yaw-axis motion simultaneously. The two four-bar linkages and the spherical six-bar linkage are designed on and built from a single piece of composite. Bending the two middle joints (② and ⑤) separately with SMA coil actuators can produce a yawing motion of the link ⓐ that connects axis ① and ⑥. Yaw motion of the mechanism produces the steering motion when each steering actuator (left, right actuator) is activated alternatively by on-off current control. A pitching motion can be produced when both middle joints are bent. The spherical six-bar linkage has 3 DOFs. Although a spherical five-bar linkage has 2 DOFs, we need a symmetrical pattern to combine the four-bar linkage on each side of the mechanism. Therefore, one more link is added, which increases the redundant DOFs. The redundant motion of the proposed spherical six-bar linkage is roll. The roll motion is twisting of link ⓐ, ⓓ. The roll angle is negligible in this application.

The trajectory of the pitching and yawing motions is determined by a kinematic equation for the pattern shown in Fig. 4. The pattern is designed using the shape-angle parameter θ. The shape angle is the angle between the horizontal and the inclined axis and determines how much the steering mechanism can turn with a single yaw bending. The geometrical equation is $\alpha_{\max} = 2\theta$, $\beta_{\max} = 180 - 2\theta$. In the previous version of the Omegabot, we used both pitching and yawing motions [19]–[21]. In the current crawling version, a spherical six-bar linkage is used to produce just the yawing motion, as the four-bar linkages produce enough pitching motion to form an omega shape.

We determined the maximum steering angle as 90° since it is theoretically impossible to turn more than 90°. In other words, if the robot tries to steer more than 90°, the friction direction at the head and tail segments loses the opposite directional components needed for crawling; neither segment slips when the actuator is activated. Therefore, the shape angle is determined to be 45°, from the geometrical equation above. The steering performance is described in the results section.

C. Anisotropic Friction Pad

The anisotropic friction pads have different friction coefficients, depending on the direction of the applied lateral force. This setup is required for the robot to crawl without an active gripper. The robot can move forward using frictional force that produces larger forward than backward force. An anisotropic friction pad is designed to change the contact material passively, depending on the direction of the lateral force. It is made of multiple beams that have a high friction coefficient polymer on one side and a low friction coefficient polymer on the other, as shown in Fig. 5. When a lateral force is applied, the beams bend and the material on one side touches the ground. If the direction of the force changes, the contact material also changes, producing different forces due to friction, depending on the direction of the lateral force.

When the robot body extends, the low friction coefficient polymer of the head segment touches the ground while the high friction coefficient polymer of the tail segment touches the ground, anchoring the tail segment and letting the head segment slip. The opposite phenomenon occurs when the robot body contracts.

We designed the beam tips to be cylindrical in shape, as shown in Fig. 5. When a beam bends, its tip rotates. If the tip is shaped like a wheel, it will maintain the tip's contact angle with the ground as the tip rotates.

D. Actuator

In this section, we describe the novel design of the LIP SMA spring actuators, where the spring is elongated to a pitch greater than 30°. Normally, SMA spring actuators are used in the region where the shape of the spring remains normal throughout the actuation. Metal springs are generally used within a pitch change of 5°, and SMA spring actuators have also been used only in this region. However, SMA actuators can be elongated much more than conventional springs and still recover their shape. Normally, the strain of SMA wire is around 5%; SMA wire actuators are used in this range. However, for SMA coil spring actuators, there is no guideline for how much elongation can be

used, considering the phase transformation. Experiments have verified that SMA can recover from a shear strain of 6% [22]. As long as the shear strain is below 6%, the deformed SMA in the martensite phase recovers its original shape in the austenite phase. Using a known stress–strain relationship, we can obtain the SMA spring design parameters that give the maximum strain when the elongation of the SMA spring reaches 6%.

The Omegabot requires two actuation states to operate: contraction and extension. It has limited volume for actuators due to its small dimensions. Considering these requirements, SMA coil actuators are suitable for the Omegabot. However, the design of these actuators is complicated due to their highly nonlinear properties and many design parameters. The force and displacement relationship of an SMA spring actuator has high hysteresis and nonlinearities in its actuation cycle because of the phase transition characteristics. These are influenced by many parameters, such as the wire diameter *d*, coil diameter *D*, number of coils *n*, and annealing temperature. Because of these complexities, the force and displacement of the SMA coil actuators have been estimated using the conventional spring equation [19]–[21]. However, because this equation does not sufficiently describe the force and displacement relationship of an SMA coil actuator, two nonlinear effects were also considered: the nonlinear detwinning effect of the SMA and the nonlinear geometric effect of the coil spring for large deformations. Experimental results and the shear strain–stress conversion equation were used to reduce the design complexity of the SMA spring actuators. The design procedure steps are as follows.

First, we select wire diameter *d* to be the smallest value available off-the-shelf. We want the spring index *C* to be as large as necessary for the maximum amount of air to be present around the wire per unit mass for cooling, which improves the actuation frequency. The spring diameter *D* is limited by the available volume for attachment and operation of the actuator. After selecting *d*, we calculate *D* using the single coil force–shear strain equation:

$$F_{\max} = \frac{\pi d^3}{8D} G_A \gamma \tag{1}$$

where G_A is the shear modulus of austenite. G_A was 18.26 GPa [22]. If *D* is larger than the limit, we use the limit value of *D*, since doing so will let us still meet the force requirement. If not, we use the calculated *D*. If *D* is such that *C* is smaller than 4, we have to increase *d* and reiterate the above process.

Second, the deflection of a single coil was determined from the maximum pitch angle. The maximum pitch angle α_f of the spring that achieves 6% shear strain was computed using parameters *d*, *D*, and *C* with the 0.06 shear strain value and including the large deformation effect of the spring geometry with the following equation:

$$\gamma = \frac{1}{C} \frac{\cos^2 \alpha_i (\sin \alpha_f - \sin \alpha_i)}{\cos^2 \alpha_f (\cos^2 \alpha_f + \sin^2 \alpha_f / (1+v))} \tag{2}$$

where *C* is the spring index (*D*/*d*), v is the Poisson's ratio, α_f is the final pitch angle, and α_i is the initial pitch angle. Assuming that the SMA is an isometric material, v is 0.33.

TABLE I
GEOMETRICAL PARAMETERS AND PROPERTIES OF SMA SPRING SPECIMENS

	Previous SMA spring (spring #1)	New LIP SMA spring (spring #2)
Designed Parameters		
Index	4.8	11
Wire diameter (*d*)	0.1 mm	0.1 mm
Spring diameter (*D*)	0.48 mm	1.1 mm
Number of coils (*n*)	20	3
Measured Data		
Mass (*m*)	20.3 mg	9.84 mg
Maximum shear strain	0.02	0.06
Maximum force (austenite) (5 mm deflection)	250 mN	150 mN
Maximum force (martensite) (5 mm deflection))	80 mN	40 mN
Maximum pitch angle	10°	29°
Cooling time (minimum value)	1 s	0.3 s
Heating time (minimum value)	0.8 s	0.4 s

Once the maximum pitch angle in the martensite phase was determined, the deflection produced by a single coil of the spring actuator could be derived using the following equation:

$$\delta = \frac{\pi n D_i}{\cos \alpha_i} (\sin \alpha_f - \sin \alpha_i). \tag{3}$$

For a required deflection, the number of coils *n* could be determined by dividing by the single coil deflection. All SMA spring design parameters (*C*, *d*, *D*, and *n*) are determined from the above procedure.

Experiments were performed to compare the differences between the new LIP SMA spring actuator and the previous version of the SMA spring actuator. The parameters and experimental data for the two types of SMA springs are described in Table I. The data show that the LIP spring actuator has a larger pitch angle and shorter cooling and heating time than the previous SMA spring.

The displacement data from the experiments were converted into shear strain using (2) and (3) to verify whether the strain of 0.06 was actually achieved, and the force data were converted into shear stress using the following equation:

$$\tau = \frac{T \times (d/2)}{J} = \frac{F \times (D/2) \times (d/2)}{(\pi d^4/32)} = \frac{8DF}{\pi d^3} = \frac{8CF}{\pi d^2} \tag{4}$$

where *J* is the polar moment of inertia, *T* is the torsion, *F* is the spring force, and *C* is the spring index (= *D*/*d*).

Fig. 6(a) shows the force and the deflection relationship from the tensile test of two kinds of SMA spring actuator in full martensite and full austenite phase. The actuation distance is the difference in deflection between the austenite curve and the martensite curve under constant force, since the actuators were arranged antagonistically. For a spring index of 4.8 and an initial length of 5.2 mm, a spring force of 9 g (88 mN) was required for the actuator to overcome the antagonistic actuators in the martensite phase and move 3 mm. However, for an index of 11, less force was required; this implies that we could reduce the force applied to the antagonistic actuators, which represents an

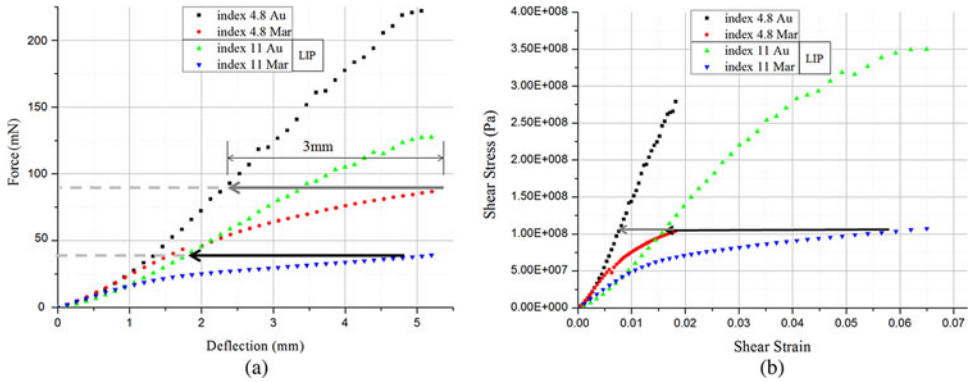

Fig. 6. (a) Experimental curve of the force–deflection relationship and (b) shear strain–shear stress curve obtained from the force–deflection data. SMA spring specimen #1 has an index of 4.8 with $d = 100$ μm, $D = 480$ μm, and $n = 20$. The black squares correspond to the austenite phase and the red dots correspond to the martensite phase. SMA spring specimen #2 has an index of 11 with $d = 100$ μm, $D = 1.1$ mm, and $n = 3$. The green triangles correspond to the austenite phase and the blue triangles correspond to the martensite phase. (Arrows: Antagonistic actuation route of the index 4.8 SMA spring actuator (gray arrow) and the index 11 (LIP) SMA spring actuator (black arrow).)

energy loss. This can be explained by the shear strain–stress curve. If we use the full detwinning region of the SMA, we can reduce the martensite SMA spring force, because the SMA is very compliant in the detwinning region.

Fig. 6(b) shows the shear stress–shear strain version of the curves. The austenite phase curve indicates a linear relationship between the shear strain and the shear stress. However, the martensite phase curve indicates a highly nonlinear relationship. As shown in the figure, SMA detwinning starts at a shear strain of 0.01. After this point, the slope of the curve decreases significantly. The tensile test of the LIP spring was done up to a shear strain of around 0.06. Beyond this point, the slope could increase, since the detwinning ends and the elastic deformation become more influential [22], [23]. The curve of the small-index SMA spring (Index 4.8) shows that the strain stops at 0.02. The force–deflection curve of the LIP SMA spring in Fig. 6(a) shows that the slope drop occurs at a shorter spring deflection than the small-index SMA spring. This shows that the LIP SMA spring uses the full compliant region of detwinning, whereas the small-index SMA spring does not. Accordingly, the differences in the stress and the strain of two phases are at a maximum when the shear strain is around 0.06. Therefore, the SMA spring should be designed so that maximum strain reaches 0.06. In summary, the SMA spring design followed three criteria. First, we set the maximum shear strain to 0.06 to maximize the difference between the stress of the austenite and martensite phases. This was required for the antagonistic actuation, which is based on the force difference between the two phases. Second, we selected the maximum spring index, taking into account any thermomechanical effects such as convection. Generally, a large spring index improves convection, which is related to SMA actuator frequency, by reducing cooling time. Third, we selected the number of spring coils that satisfied the actuator stroke and maximum strain requirements.

We selected an SMA spring with an index of 11 as the Omegabot's actuator. This spring is small enough to fit in the Omegabot and provides a strain of 0.06 for a 3-mm actuation length by antagonistic actuation. The spring actuator should be attached to the upper part of the bending segment when it is bent by 60° and to the lower part of the bending segment when it is bent by 120°, after it elongates the spring by 5 mm. This will produce the 3-mm difference between the activated SMA spring (Au) and the nonactivated SMA spring (Mar), which is the displacement generated by the antagonistic actuator. This is verified in the experimental results shown in Fig. 6(a). The thin-film joint stiffness is negligible compared with that of the SMA spring actuator and so it is not considered. Finally, the entire SMA spring actuator length, which is the distance between the soldering spot on the bending segments, is 25 mm. Design of the steering actuators follows the same procedure as the design of the actuators for the crawling motion. The coil diameter D and the wire diameter d are the same with the actuators for crawling. Two actuators (left, right) have enough force to elongate each actuator when one is activated (heated) and the other is deactivated (cooled). The coil number is determined by the required displacement. To fully fold the steering mechanism, it requires 15 mm of displacement. However, since the initial coil length is about 1 mm, it is designed to produce 14 mm of displacement, which requires a total of 14 coils.

III. Fabrication

A. Body Structure

The Omegabot's entire body structure was designed on a 2-D pattern. The flat four-bar linkages and folding spherical six-bar linkage design enable fabrication of the robot structure on a single piece of composite. The robot body structure can be built by laser cutting and a single curing process and does not require any assembly. With this simple design, mass production using one piece of composite is possible. Fig. 7(a) shows that three robot bodies can be fabricated during a single manufacturing cycle.

The robot body is made from composites consisting of glass fibers and copper-laminated Kapton film (Dupont Co.). This fabrication process using composites and flexure joints was introduced by Wood *et al.* [13] and is suitable for small-scale robots due to the low friction loss and integrated circuit manufacturing it entails. We actuate the link and joint structure with

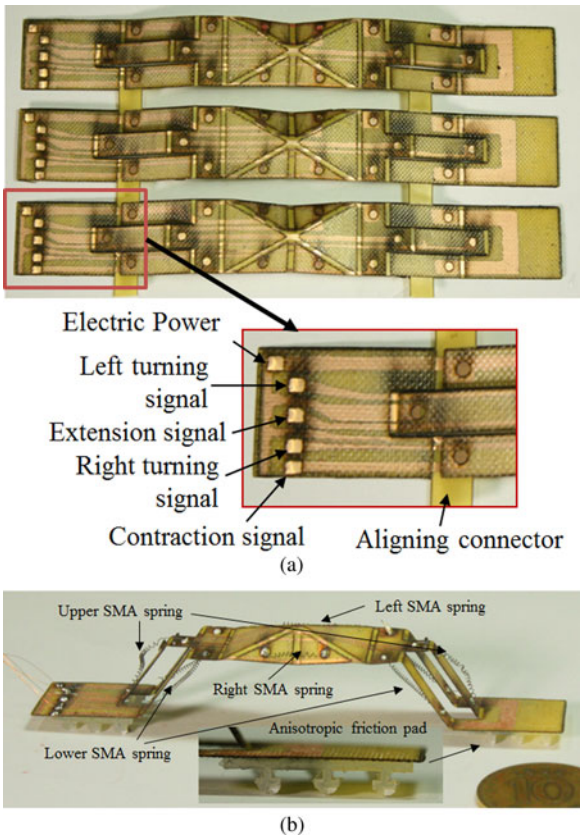

Fig. 7. (a) Three robot bodies made from a single piece of composite and embedded wiring. (b) Final Omegabot prototype with SMA spring actuators and anisotropic friction pads.

SMA spring actuators acting as artificial muscles. A small-scale robot can be built from this structure, as described by Cho *et al.* [17].

SMA spring actuators and anisotropic friction pads are attached to the body structure, as described in the previous section. Fig. 7(b) shows the final prototype of the Omegabot. The SMA spring actuators are soldered to the body, and the anisotropic friction pads are glued under the head and the tail segments. Two pads are glued to each segment; each pad consists of three beams.

B. Anisotropic Friction Pad

The anisotropic friction pad is fabricated using the molding process shown in Fig. 8. The molding process is suitable for making parts out of soft material [23]. The 5-mm-thick acryl panel is cut into patterned shapes using a laser cutter (Universal Laser M-300, CO_2 laser). The small mold for the rigid part (Smooth Cast 300, SmoothOn, Co.) has an arched shape, a width of 1 mm, and a height of 0.5 mm. Most of the pad is made from soft material (Dragonskin, SmoothOn, Co.). The beam width t and height L are 0.5 and 1 mm, respectively. The beam can be bent during the robot's inchworm motion, and the contact material changes as the direction of the force changes.

Fig. 9 shows measurements of the maximum static friction force for each lateral force direction under varying normal force.

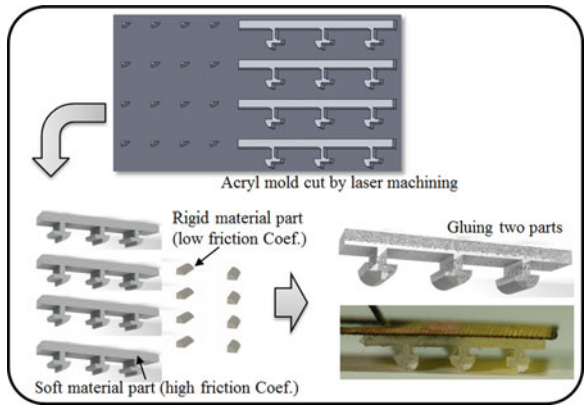

Fig. 8. Molding process to make an anisotropic friction pad.

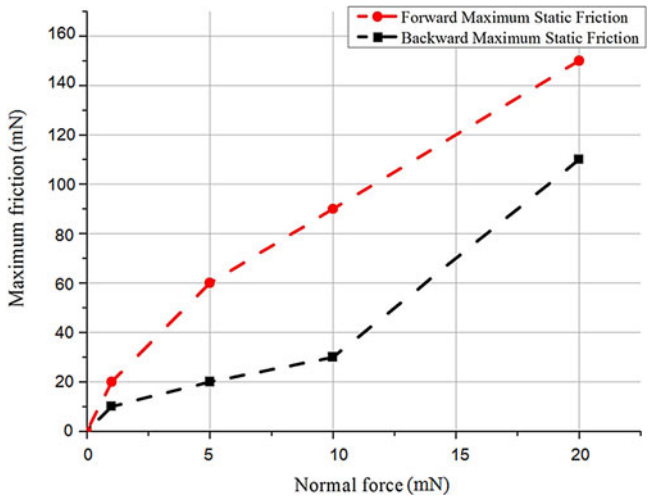

Fig. 9. Friction in different directions for various normal forces. The slope of the graph gives the friction force coefficient.

The forward friction was three times higher than the backward friction when the normal force was less than 10 mN. When the normal force was greater than 10 mN, the anisotropic friction pads did not work well because the polymer beams were bent too much and the high friction material contacted the ground regardless of the direction of the lateral force. Because the weight of Omegabot is less than 10 mN, assuming that the battery and control circuits are embedded, the anisotropic friction pad produced three times larger forward force than the backward force.

C. SMA Spring Actuator

The SMA spring was fabricated by winding the SMA wire (Dynalloy Co.) around a core wire with a drilling machine and annealing it after clamping both ends [25]. This process can be used to make SMA spring actuators with a large number of coils. However, we require SMA spring actuators with a specific number of coils and specific lengths of straight wires at both ends. The straight wires determine the initial length of the spring when it is soldered on the robot body and are required for the actual soldering. For manufacturing purposes, each actuator

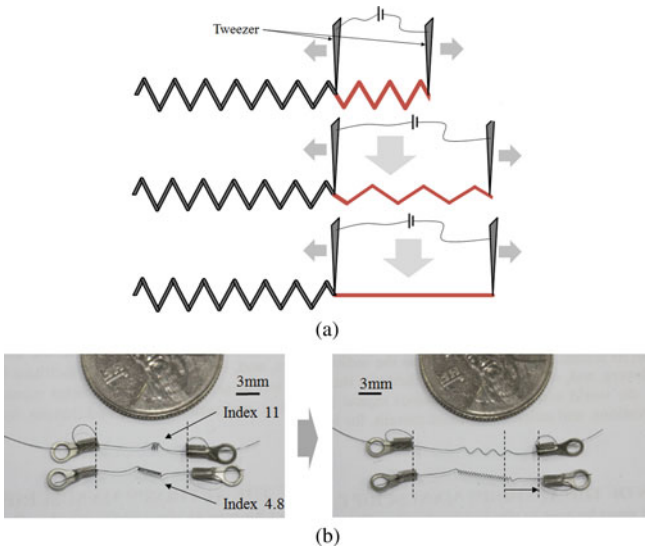

Fig. 10. (a) Reannealing process for uncurling the coil. (b) Two SMA spring specimens (index of 11 and 4.8). Note that the crimps on the ends of the actuators are for testing; in the robot, the SMA springs are soldered directly without crimping.

TABLE II
SPECIFICATIONS OF THE CRAWLING OMEGABOT

Dimension	
Length	150 mm
Width	15 mm
Height	34 mm (maximum)
Weight	
Body structure weight	0.8 g
SMA actuator weight	0.03 g
Anisotropic friction pads	0.3 g
Total weight (including solder, etc.)	1.2 g

requires a separate core and separate clamps before it is put into a furnace for annealing at high temperatures for about an hour. This presents a challenge for mass-producing these actuators. It is easier to anneal a single long actuator than many separately clamped actuators. Therefore, we developed a method of using one long SMA spring actuator for manufacturing. We cut the long SMA spring actuator to the desired length and uncurled the coils except for those needed for the actuation. The coils at the end of the spring were uncurled through a second annealing process using electric conductive tweezers and a power supply after the extra coils were stretched. Applying a high current reannealed the coils and straightened the wire, as shown in Fig. 10(a). With this process, we could quickly obtain a spring with the desired number of coils from one long SMA spring actuator coil, as seen in Fig. 10(b). This figure shows that the LIP SMA spring has large pitch angle and contains more air for convection than the small-index SMA spring actuator as described in the design section.

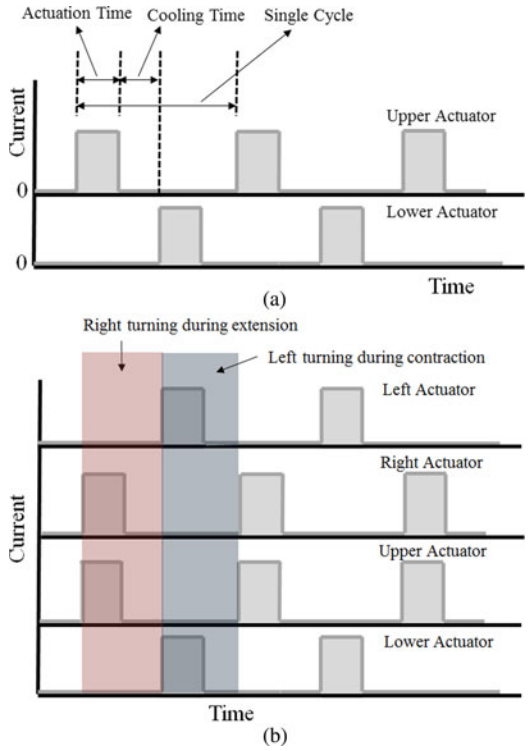

Fig. 11. (a) Current input pattern for crawling motion. The upper and lower actuators are used to extend and contract the body antagonistically. (b) Current input pattern for steering motion.

IV. RESULTS AND DISCUSSION

A prototype of the robot was built with the design described in the previous section. Two types of actuators, a small-index SMA spring actuator and an LIP SMA spring actuator, were tested to demonstrate the improved performance of the LIP SMA spring actuator. The specifications of the Omegabot are shown in Table II. The weight of each part was measured with a balance. The length of the body was 150 mm (two foot segments of 35 mm, two bending segments of 25 mm, and one steering segment of 30 mm); the weight of the body, including the actuators and the anisotropic friction pads, without any power, was 1.2 g. We added weight to the head and the tail segments to emulate the battery and control circuit. The anisotropic friction pads were designed to work under the weight of the battery and circuits: if the robot is too light, the beams on the pad will not bend, and if it is too heavy, the beams will bend too much. The details of the robot's weight are listed in Table II. The robot was tested on a piece of white paper to aid visibility. The robot was controlled by an open loop on/off control; 0.35-A current was applied to each actuator for heating and no current was applied for cooling. The ratio of heating and cooling time was the duty ratio of a single actuation.

For crawling, the upper SMA spring and the lower SMA spring were activated alternately, as shown in Fig. 11(a). The upper actuator extended the body while the lower actuator contracted the body into an omega shape. Both actuators were actuated for the same actuation time. To avoid activating both actuators at the same time, the cooling time was defined as

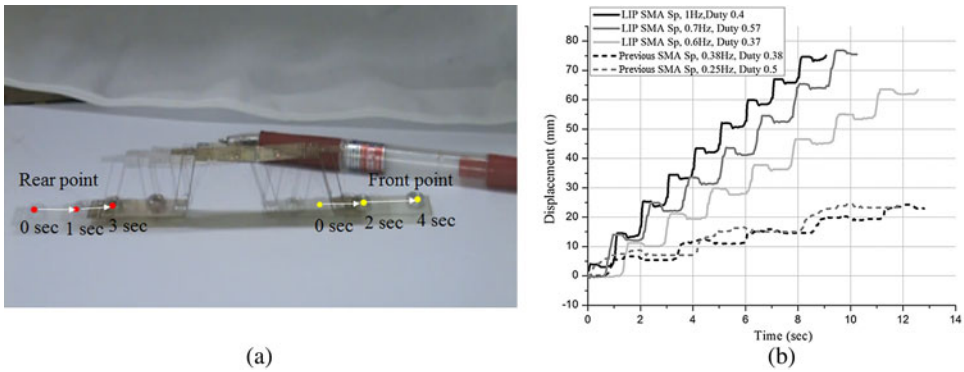

Fig. 12. (a) Crawling motion snapshot (1-s intervals). (b) Trajectory of the front of the crawling robot.

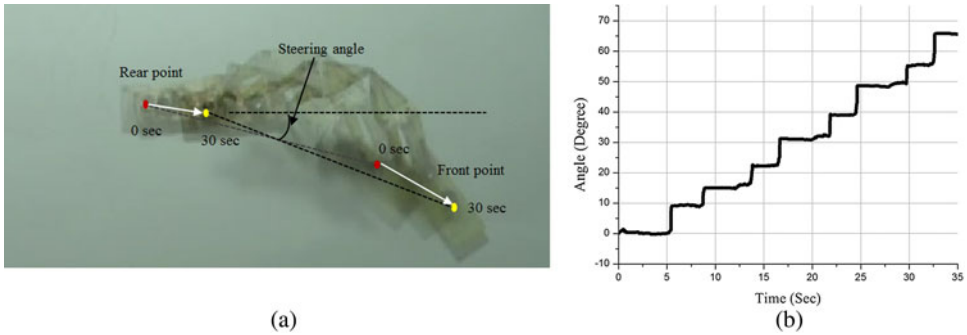

Fig. 13. (a) Steering motion snapshot (30-s interval). (b) Steering angle while the robot is turning.

the duration that both actuators were not activated and was always larger than zero. The period of actuation was twice the sum of the actuation time and cooling time. The crawling experiments were performed with various actuation and cooling times, varying between 0.1 and 5.0 s and with actuation frequencies between 0.1 and 2.0 Hz. However, actuation frequency is limited during crawling: the robot cannot move at a high frequency because cooling time will not be sufficient to extend the SMA spring actuator. The maximum speed of the robot was 9 mm/s, and the maximum stride length was 25 mm, whereas the maximum actuation frequency was 1 Hz.

For steering, the robot needs to turn and move forward at once. Two more actuators on both sides of the steering mechanism need to be activated. Input signals to the four actuators, right, left, upper, and lower actuators, for steering the body right are shown in Fig. 11(b). For the body to turn, the tail segment has to be anchored and the head segment has to be able to move freely. To anchor the tail segment, the robot body has to extend. Therefore, to steer right, the right actuator turns on to bend the body to the right side, while the upper actuator turns on to extend the body; the head segment moves forward while turning right. After the head segment has moved forward and right, the tail segment has to be pulled in left of the body, while the head segment remains in place. Therefore, the left actuators turn on at the same time with the lower actuator turning on to contract the robot body.

Fig. 12(a) shows an overlapped snapshot of a series of images taken at 1-s intervals while the robot was crawling. The test was performed using the LIP SMA spring actuators. Captured motion data for five tests were obtained using a video analysis program (Proanalyst), as shown in Fig. 12(b). Three of the tests were for a robot with the LIP SMA spring actuators with an index of 11, and two were for a robot with a previous version of SMA spring actuators with an index of 4.8. The LIP SMA actuator could be driven up to 1 Hz, whereas the previous version of SMA spring actuator could only be actuated up to 0.38 Hz. The plot shows that the crawling speed was improved by using the LIP SMA spring actuators. Different actuation duty ratio affects the stride length and the speed. Lower duty ratio means that the activation time is shorter. Therefore, the stride length of the robot is reduced compared with what happens at a similar frequency, and the speed decreases. Each step shows the movement of the head segment for each actuation cycle. The curves decreased slightly after each step, showing the effect of slippage caused by the pad slipping when the soft high-friction material touched the ground.

The average speed of the robot can be found by calculating the average stride length from the graph and multiplying it by the actuation frequency. For the LIP SMA actuators, a lower actuation frequency resulted in a larger stride length but a lower speed. The robot speed was proportional to both the frequency and the stride length; however, as the frequency increased, the stride length decreased. Therefore, there is a certain maximum robot speed as the actuation frequency increases.

Overlapping snapshots of steering using the two-anchor motion are shown in Fig. 13(a). The steering angle was measured by connecting a line between a point on the head segment and a point on the tail segment and measuring the change in the angle

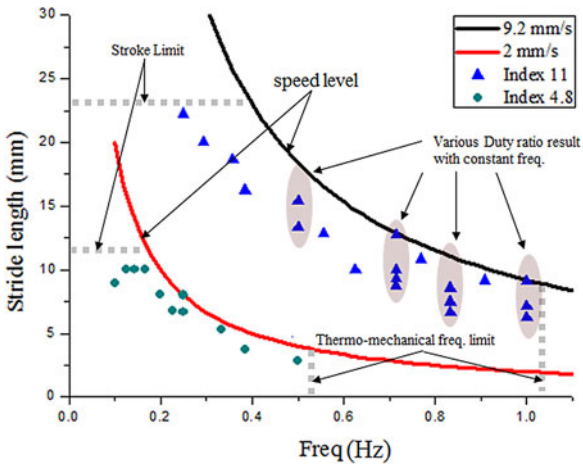

Fig. 14. Frequency and the stride length of the crawling Omegabot actuated by two kinds of SMA spring actuator, index 11 (blue triangle dot), index 4.8 (green dot). The experiments were performed with various frequency and duty ratio (activation time:cooling time) of current control. Two inverse proportion curves (black 9.2 mm/s, red line 2 mm/s) indicate the constant velocity line.

of this line. Fig. 13(b) shows a plot of the steering angle with time as the robot steered to the right at 110°/min. In the graph, we can observe that the angle and time per step were not constant. The robot is controlled by the on-off forward control. The condition of the ground surface varied and unpredictable stiction of the anisotropic friction pad occurred. For these reasons, it was hard to maintain a constant steering angle.

Experimental results of crawling obtained using the two types of SMA spring actuators are plotted on a single figure in Fig. 14 with actuation frequency on the *x*-axis and stride length on the *y*-axis to evaluate various actuation and cooling times. The stride length of the robot was measured by tracking the position of the head segment during a single actuation cycle. The speed of the robot was calculated by multiplying stride length by actuation frequency. Each test is shown by a single point on the graph. A line of constant speed can also be plotted on the graph to compare the speed of the robot for different actuation frequency and duty ratio; the experiments were conducted while changing the actuation frequency from 0.1 to 2 Hz and duty ratio from 10% to 90%. The graph shows the highest speed result at each frequency. In addition, for some frequencies, several points that are the results of a different duty ratio for the same frequency are plotted as well.

The plot shows two groups of data: one (bottom left) corresponds to the robot with small-index SMA spring actuators (used in the previous version of the robot), and the other (top right) corresponds to the robot with LIP SMA spring actuators. Various actuation and cooling times were tested for each robot. The upper line represents the maximum speed of the robot with LIP SMA spring actuators, and the lower line represents the maximum speed of the robot with small-index SMA spring actuators. The constant speed lines are inversely proportional curves because the speed is a product of actuation frequency and stride length. The speeds of the robot using LIP SMA spring actuators were distributed on the higher line for two reasons. First, the LIP SMA spring had a much lower force during the martensite phase, which means that the antagonistic actuator could pull the linkage easier, increasing the maximum stride length. Second, the LIP SMA spring had improved cooling performance because more surrounding air was used for cooling, allowing the LIP SMA spring actuator to cool faster, thereby increasing the maximum actuation frequency.

As shown in Fig. 14, increasing the frequency reduced the stride length, but the speed of the robot did not change drastically. This means that the relationship between the actuation frequency and the stride length of the robot was nearly inversely proportional. At a high frequency, the antagonistic actuators did not have enough time to produce the full actuation stroke, but the average robot speed was maintained. However, there was a thermomechanical limit for the actuation frequency, above which the actuators did not move. When the actuation frequency exceeded this value, the SMA spring did not have enough cooling time for elongation, and the opposite actuator could not pull the linkage. In addition, there is a duty ratio limit. When the input current had a low duty ratio, the SMA spring did not have enough heating time for activation, and the actuator could not pull the linkage. A stroke limit was imposed by the SMA spring maximum actuation distance. The LIP SMA spring actuator had a high stroke limit because the spring design reduced the opposing actuation force.

The robot was tested on an uneven surface, such as a keyboard. The anisotropic friction pads were effective and the robot was able to travel across it. The beams in the anisotropic friction pads provided adaptable contact characteristics.

V. Conclusion and Future Work

In this paper, we have presented a novel design concept for a small-scale robot inspired by an inchworm, along with an analysis for improving the performance of the proposed robot. All the mechanisms were designed as 2-D patterns on a single piece of composite and were folded into working mechanisms without the need for assembly. A novel design concept of an LIP SMA spring actuator was also presented to improve the performance of the SMA spring actuators. The spring index and pitch angle range of the actuators were increased in order to increase the actuation frequency and stroke of the actuators.

The robot body structure was fabricated on the basis of a single-layer patterning design. The single-piece robot body contained two four-bar linkages for two-anchor crawling and a spherical six-bar linkage for steering. The design was based on composite structures and a flexure joint that can be fabricated using suitable manufacturing processes for small-scale robots. We focused on the crawling and steering motions that allowed the robot to move in a 2-D plane using anisotropic friction pads, although real inchworms move in 3-D space using prolegs. The robot's agility was also demonstrated.

The LIP SMA spring actuators improved the actuation performance at high frequencies, providing better cooling and increasing stride length by reducing the opposing force of the antagonistic actuation. A large spring index was effective for cooling because it ensured that more air was contained in the same mass of the spring coil, resulting in an improved actuation

frequency during cyclic actuation of the SMA spring actuators. A large pitch during the martensite phase indicated that the SMA spring was in a compliant region. This led to detwinning of the martensite phase, which reduced the slope of the stress–strain curve, elongated the actuator, and increased the actuation distance for a given force during antagonistic actuation.

The LIP SMA spring actuator is not a specific type of the actuator but a design method to determine the parameters of the optimal SMA coil spring actuator. It is helpful for the microscale mechanical systems that use the SMA coil spring actuator for cyclic linear actuation since this SMA design procedure enhances the SMA actuation frequency and the energy efficiency.

For future work, the crawling and steering speed can be improved by developing a control algorithm for steering and by optimizing the anisotropic friction pad design. By including a small-scale gripper, the robot can grip the surface and move over various terrains in a 3-D space, including vertical climbing and slope transition crawling. A normalized inchworm locomotion analysis can be performed to optimize the efficiency and performance of an inchworm robot. Modeling of the SMA spring actuator by considering a thermomechanical model and SMA hysteresis characteristics is required to control the robot more precisely. Although it has various limitations, this lightweight crawling robot has potential for use in hazardous areas where there is a need for sensing and reconnaissance.

REFERENCES

[1] T. M. Casey, "Energetics of caterpillar locomotion: Biomechanical constraints of a hydraulic skeleton," *Science*, vol. 252, no. 5002, pp. 112–114, Apr. 1991.

[2] B. A. Trimmer, A. Takesian, B. Sweet, C. B. Rogers, D. C. Hake, and D. J. Rogers, "Caterpillar locomotion: A new model for soft-bodied climbing and burrowing robots," in *Proc. 7th Int. Symp. Technol. Mine Problem*, 2006, pp. 1–10.

[3] A. Menciassi, D. Accoto, S. Gorini, and P. Dario, "Development of a biomimetic miniature robotic crawler," *Autonom. Robots*, vol. 21, pp. 155–163, 2006.

[4] J. Zuo, G. Yan, and Z. Gao, "A micro creeping robot for colonoscopy based on the earthworm," *J. Med. Eng. Technol.*, vol. 29, no. 1, pp. 1–7, 2005.

[5] K. Wang, G. Yan, G. Ma, and D. Ye, "An Earthworm-like robotic endoscope system for human intestine: Design, analysis, and experiment," *Ann. Biomed. Eng.*, vol. 37, no. 1, pp. 210–221, Jan. 2009.

[6] B. Kim, S. Park, C. Y. Jee, and S. J. Yoon, "An earthworm-like locomotive mechanism for capsule endoscopes," in *Proc. Conf. IEEE/RSJ Int. Conf. Intell. Robots Syst.*, Aug. 2015, pp. 2997–3002.

[7] J. Brackenbury, "Caterpillar kinematics," *Nature*, vol. 390, no. 6659, p. 453, Dec. 1997.

[8] K. Kotay and D. Rus, "The inchworm robot: A multi-functional system," *Auton. Robots*, vol. 8, no. 1, pp. 53–69, Jan. 2000.

[9] W. Wang, Y. Wang, K. Wang, H. Zhang, and J. Zhang, "Analysis of the kinematics of module climbing caterpillar robots," in *Proc. IEEE/ASME Int. Conf. Adv. Intell. Mechatronics*, Jul. 2008, pp. 84–89.

[10] N. Lobontiu, M. Goldfarb, and E. Garcia, "A piezoelectric-driven inchworm locomotion device," *Mech. Mach. Theory*, vol. 36, no. 4, pp. 425–443, Apr. 2001.

[11] H. Lin, G. Leisk, and B. Trimmer, "GoQBot: A caterpillar-inspired soft-bodied rolling robot," *Bioinspiration Biomimetics*, vol. 6, p. 026007, Jun. 2011.

[12] M. S. Kim, W. S. Chu, J. H. Lee, Y. M. Kim, and S. H. Ahn, "Manufacturing of inchworm robot using shape memory alloy (SMA) embedded composite structure," *Int. J. Precis. Eng. Manuf.*, vol. 12, no. 3, pp. 565–568, 2011.

[13] R. J. Wood, S. Avadhanula, R. Sahai, E. Steltz, and R. S. Fearing, "Microrobot design using fiber reinforced composites," *J. Mech. Des.*, vol. 130, p. 052304, 2008.

[14] R. J. Wood, "The first takeoff of a biologically inspired at-scale robotic insect," *IEEE Trans. Robot.*, vol. 24, no. 2, pp. 341–347, Apr. 2008.

[15] M. Noh, S. Kim, S. An, J. Koh, and K. Cho, "Flea-inspired catapult mechanism for miniature jumping robots," *IEEE Trans. Robot.*, 2012, to be published. Available: http://ieeexplore.ieee.org/xpls/abs_all.jsp?arnumber=6204349.

[16] K. Cho and H. H. Asada, "Architecture design of a multiaxis cellular actuator array using segmented binary control of shape memory alloy," *IEEE Trans. Robot.*, vol. 22, no. 4, pp. 831–843, Aug. 2006.

[17] K. Cho, E. Hawkes, C. Quinn, and R. J. Wood, "Design, fabrication and analysis of a body-caudal fin propulsion system for a microrobotic fish," in *Proc. IEEE Int. Conf. Robot. Autom.*, May 2008, pp. 706–711.

[18] A. M. Hoover, E. Steltz, and R. S. Fearing, "RoACH: An autonomous 2.4g crawling hexapod robot," in *Proc. IEEE Int. Conf. Robot. Autom.*, Sep. 2008, pp. 26–33.

[19] J. Koh and K. Cho, "Omegabot: Biomimetic inchworm robot using SMA coil actuator and smart composite microstructures (SCM)," in *Proc. IEEE Int. Conf. Robot. Biomimetics*, Dec. 2009, pp. 1154–1159.

[20] J. Koh and K. Cho, "Omegabot: Crawling robot inspired by *Ascotis Selenaria*," in *Proc. IEEE Int. Conf. Robot. Autom.*, May 2010, pp. 109–114.

[21] J. Koh, S. An, and K. Cho, "Finger-sized climbing robot using artificial proleg," in *Proc. IEEE/RAS Int. Conf. Biomed. Robot. Biomechatronics*, Sep. 2010, pp. 610–615.

[22] S. Ahn, J. Ryu, M. Cho, and K. Cho, "Engineering design framework for a shape memory alloy coil spring actuator using a static two-state model," *Smart Mater. Struct.*, vol. 21, no. 5, p. 055009, May 2012.

[23] Y. Toi, J. Lee, and M. Taya, "Finite element analysis of superelastic, large deformation behavior of shape memory alloy helical springs," *Comput. Struct.*, vol. 82, no. 20–21, pp. 1685–1693, Aug. 2004.

[24] K. J. Cho, J. S. Koh, S. Kim, W. S. Chu, Y. Hong, and S. H. Ahn, "Review of manufacturing processes for soft biomimetic robots," *Int. J. Precis. Eng. Manuf.*, vol. 10, pp. 171–181, Oct. 2009.

[25] S. Kim, E. Hawkes, K Cho, M. Joldaz, J. Foleyz, and R. Wood, "Micro artificial muscle fiber using NiTi spring for soft robotics," in *Proc. IEEE/RSJ Int. Conf. Intell. Robots Syst.*, Oct. 2009, pp. 2228–2234.

Je-Sung Koh (S'10) received the B.S. degree in mechanical and aerospace engineering from Seoul National University, Seoul, Korea, in 2008, where he is currently working toward the Ph.D. degree in the Biorobotics Laboratory.

His current research interests include bioinspired robot design and small-scale robot design with smart materials.

Mr. Koh received the Best Student Paper Award at the IEEE/RSJ EMBS International Conference on Biomedical Robotics and Biomechatronics in 2010.

Kyu-Jin Cho (M'08) received the B.S and M.S. degrees from Seoul National University, Seoul, Korea, in 1998 and 2000, respectively, and the Ph.D. degree in mechanical engineering from the Massachusetts Institute of Technology, Cambridge, in 2007.

He was a Postdoctoral Fellow at the Harvard Microrobotics Laboratory until 2008. He is currently an Assistant Professor of Mechanical and Aerospace Engineering and the Director of the Biorobotics Laboratory, Seoul National University. His research interests include biologically inspired robotics, robotics systems using smart actuators, novel mechanisms using smart structures, and rehabilitation and assistive robotics.